Antarctic Bottom Water warming and freshening: Contributions to sea level rise, ocean freshwater budgets, and global heat gain*

SARAH G. PURKEY[1,2,3] and GREGORY C. JOHNSON[2,1]

[1]*School of Oceanography, University of Washington, Seattle WA 98195, USA*

[2]*NOAA/Pacific Marine Environmental Laboratory, Seattle WA 98115, USA*

for *Journal of Climate*

draft 26 November 2012

* Pacific Marine Environmental Laboratory Contribution Number 3954

[3]*Corresponding author address*: Sarah G. Purkey, School of Oceanography, Box 357940, University of Washington, Seattle WA 98195-7940, USA. E-mail: sarah.purkey@noaa.gov.

Abstract:

Freshening and warming of Antarctic Bottom Water (AABW) between the 1980s and 2000s are quantified, assessing the relative contributions of water-mass changes and isotherm heave. The analysis uses highly accurate, full-depth, ship-based, conductivity-temperature-depth measurements taken along repeated oceanographic sections around the Southern Ocean. Fresher varieties of AABW are present within the South Pacific and South Indian oceans in 2000s compared to the 1990s, with the strongest freshening in the newest waters adjacent to the Antarctic continental slope and rise indicating a recent shift in the salinity of AABW produced in this region. Bottom waters in the Weddell Sea exhibit significantly less water-mass freshening than those in the other two southern basins. However, a decrease in the volume of the coldest, deepest waters is observed throughout the entire Southern Ocean. This isotherm heave causes a salinification and warming on isobaths from the bottom up to the shallow potential temperature maximum. The water-mass freshening of AABW in the Indian and Pacific sectors is equivalent to a freshwater flux of 73 ±26 Gt yr^{-1}, roughly half of the estimated recent mass loss of the West Antarctic Ice Sheet. Isotherm heave integrated below 2000 m and south of 30 °S equates to a net heat uptake of 34 ±3 TW of excess energy entering the deep ocean from deep volume loss of AABW and 0.37 ±0.15 mm yr^{-1} of Sea Level Rise from associated thermal expansion.

1. Introduction

Antarctic Bottom Water (AABW) is the Southern Ocean's coldest, densest water mass. It ventilates the lower limb of the Meridional Overturning Circulation (MOC; e.g. Lumpkin and Speer 2007), filling most of the world's deep basins (Johnson 2008). In recent decades AABW has warmed (e.g. Purkey and Johnson 2010; hereafter P&J 2010), freshened (e.g. Johnson et al. 2008; Swift and Orsi 2012), and decreased in volume (e.g. Kouketsu et al. 2011; Purkey and Johnson 2012, hereafter P&J 2012), possibly linked to the increase in the glacial melt fresh water fluxes into AABW formation regions around Antarctica (e.g. Jacobs and Guilivi 2010). The freshening decreases the salinity of the shelf waters, thence AABW, and appears to slow AABW production and thus the lower limb of the MOC. Here we examine AABW property changes throughout the Southern Ocean, separating the component owing to θ–S (potential temperature–salinity) changes from that due to changes in the depth of potential isotherms (heave). We further evaluate their contributions to local sea level rise (SLR), freshwater, and heat budgets.

AABW is a combination of very cold and relatively fresh water formed on shallow continental shelves and warmer, saltier offshore Circumpolar Deep Water (CDW; Foster and Carmack 1976). The shelf waters form over shallow ice-covered continental shelves where brine rejection from sea ice formation and export increases the salinity of surface waters. This water sinks, mixing with adjacent CDW, and circulates under the ice shelf, melting the overlying ice at depth, causing the shelf waters to freshen (Jacobs 2004). These processes result in a reservoir of

52 very cold, dense shelf water that, when it leaves the shelf, flows down the
53 continental slope, further mixing with CDW (Jacobs 2004).
54 AABW formation occurs in the Ross Sea, Adelie Coast, and Weddell Sea,
55 producing three distinct varieties of AABW (Orsi et al. 1999): Ross Sea Bottom
56 Water (RSBW), Adelie Land Bottom Water (ALBW), and Weddell Sea Bottom Water
57 (WSBW). These water masses mix with overlying CDW in the Antarctic Circumpolar
58 Current (ACC) before feeding into the lower limb of the MOC and traveling to the
59 northern ends of the Pacific, West Atlantic, and Indian oceans (Johnson 2008).
60 AABW is often defined as water with neutral density $\gamma_n > 28.27$ kg m^3 found south of
61 the SubAntarctic Front (SAF; Orsi et al. 1999). Here we use an older definition for
62 AABW of deep Southern Ocean waters of $\theta < 0°C$ (e.g. Gordon 1972), because we use
63 θ, rather than γ_n, as a vertical coordinate.
64 AABW freshening has been observed (Aoki et al. 2005; Jacobs and Giulivi 2010;
65 Swift and Orsi 2012) and slowdown of AABW formation rates inferred (P&J 2012) in
66 the Ross Sea and Australian-Antarctic Basin starting as early as the 1950s. Ross Sea
67 Shelf Water, an important constituent of RSBW, has freshened by 0.03 $decade^{-1}$
68 between 1958 and 2008, associated with freshening of the coastal current
69 connecting the Amundsen Coast to the Ross Sea Shelf (Jacobs and Giulivi 2010).
70 Along the west side of the Ross Gyre, within the deep western boundary current
71 transporting the recently formed RSBW northwestward, the densest water seen in
72 1994 completely disappeared by 2011, the deep and surface constituents of the
73 shelf water freshened, and thickness of the RSBW outflow decreased by a few
74 hundred meters (Swift and Orsi 2012). Directly downstream from its formation

region in the Australian-Antarctic Basin, ALBW has freshened by 0.03 between 1994 and 2002 (Aoki et al. 2005). In the deep Australian-Antarctic Basin, ventilated by both RSBW and ALBW, freshening is evident throughout the basin, owing either to fresher bottom water or different ratios of RSBW and ALBW (Whitworth III 2002; Rintoul 2007; Johnson et al. 2008). In both the Australian-Antarctic Basin and the Ross Sea, cooling on isopycnals and warming on isobars are also present (Aoki et al. 2005; Johnson et al. 2008; Jacobs and Guilivi 2010; P&J 2010).

In the Weddell Sea, bottom water and deep water have been warming with little change in salinity (Robertson et al. 2002; Fahrbach et al. 2004; 2011; P&J 2010). To the north, the deep waters in the Scotia Sea and Argentine Basin, both directly fed by WSBW, have warmed and decreased in volume for at least the past three decades (Coles et al. 1996; Johnson and Doney 2006; Meredith et al. 2008; P&J 2012).

Outside the Southern Ocean, AABW has warmed around the globe (P&J 2010; Kouketsu et al. 2011). The global-scale warming could be caused by a decrease in AABW formation rates, causing isopycnals to fall, hence the observed warming on isobaths. This signal can be communicated remotely by planetary waves throughout the world ocean on much shorter time scales than advective changes (Masuda et al. 2010; Kouketsu et al 2011; P&J 2012). AABW warming has been analyzed in the Western South Atlantic (Johnson and Doney 2006; Zenk and Morozov 2007), throughout the Pacific (Fukasawa et al. 2004; Johnson et al. 2007; Kawano et al. 2010) and in the eastern Indian Ocean (Johnson et al. 2008; P&J 2010).

97 Much of the recent AABW property changes observed around the globe may be
98 owing to increased glacial freshwater discharge from a number of locations around
99 Antarctica over recent decades (e.g. Jacobs and Guilivi 2010). Antarctic ice shelf
100 thinning and glacial discharge acceleration are strongest along the West Antarctic
101 Peninsula and the Amundsen Coast (Rignot and Jacobs 2002; Rignot et al. 2008).
102 with a net ice sheet loss of 88 ±54 Gt yr^{-1} in the West Antarctic and 60 ±46 Gt yr^{-1}
103 along the peninsula between 1992–2006 (Rignot et al. 2008). Between 1991 and
104 2001 154 ±16 km^3 of glacier ice was lost to the Amundsen Sea with acceleration of
105 coastward glacier flow (Shepherd et al. 2002). At Pine Island Glacier, a location with
106 one of the highest melt rates, the ice shelf has recently been thinning at a rate of 5.5
107 m yr^{-1} through basal melting owing to a 0.5 °C warming of ocean waters under the
108 ice shelf (Shepherd et al. 2004). Similarly, along the Amundsen and Bellingshausen
109 coasts where warm CDW has access to the shelf, the melting rates on the submerged
110 undersides of glaciers have been correlated with warming ocean temperatures, with
111 melting increasing by 1 m per 0.1 °C of warming (Rignot and Jacobs 2002).
112 The observed AABW property and circulation changes are important for global
113 heat and SLR budgets (P&J 2010; Kouketsu et al 2011). The deep ocean warming
114 below 4000 m globally is equivalent to a net heat uptake of 0.027 ±0.009 W m^{-2} over
115 the surface the Earth and 0.05 mm yr^{-1} mean global SLR (P&J 2010). In the Southern
116 Ocean, the warming below 1000 m is equivalent to as much as a 1.2 W m^{-2} local heat
117 flux and 1.3 mm yr^{-1} local SLR (P&J 2010).
118 Here we evaluate salinity and temperature changes within the deep Southern
119 Ocean, distinguishing between heave and water property changes. Section 2

discusses the data set and processing, including inter-cruise salinity adjustments (see also Appendix A). Section 3 presents methods used to distinguish heave from water-mass changes. Section 4 discusses freshening trends throughout the Southern Ocean, using several Southern Ocean sections occupied multiple times since the 1980s. Section 5 estimates basin-mean rates of change to find the contributions of the deep Southern Ocean to changes in SLR, heat budgets and freshwater budgets. Section 6 discusses these results.

2. Data and Processing

We use full-depth, high-resolution, highly accurate, ship-based hydrographic data collected in the Southern Ocean since 1980 at locations with two or more occupations. The data were mostly collected as part of the international World Ocean Circulation Experiment (WOCE) Hydrographic Programme or the Global Ocean Ship-based Hydrographic Investigation Program (GO-SHIP). All publicly available data at http://cchdo.ucsd.edu as of November 2012 are considered here. We refer to each section by its WOCE ID (Fig. 1, Table A1). All data collected along a section within a year are combined and referred to as a single occupation of that section, referenced by the calendar year in which the earliest station was taken (Table A1).

We focus on sections located at or south of 30 °S (Fig. 1): nine meridional sections roughly spaced every 45º longitude, two zonal sections at ~67 °S across the Ross Sea and the Weddell Sea, and three zonal sections that together completely circumnavigate the globe near 30 °S (Fig. 1). Most of the meridional sections in the

143 Indian and Atlantic sectors extend to the Antarctic continental shelf, but both of the
144 sections in the Pacific sector stop short of the shelf (Fig. 1). Along each section data
145 were collected from the surface to approximately 10 m from the bottom at stations
146 nominally spaced every 55 km. Each section has been occupied between 2 and 8
147 times with the length-weighted mean and median for the study region of 3.6 and 3
148 occupations, respectively (Table A1). The length-weighted mean first occupation
149 occurred in 1991 and the last in 2008. Therefore along section trends discussed
150 here span on average an 18-year period (Table A1). Each re-occupation of a given
151 section considered is within 10 km of the original. Data along each section are
152 interpolated onto an evenly spaced 20-dbar vertical and 2' horizontal grid following
153 P&J (2010).

154 All data were collected with a Conductivity-Temperature-Depth (CTD)
155 instrument with target measurement accuracy better than 0.002 °C for temperature,
156 3 dbar for pressure, and 0.002 PSS-78 for salinity (Joyce 1991). All CTD
157 temperature data were reported in, or converted to, the 1968 International Practical
158 Temperature Scale (IPTS-68) for use with the 1980 Equation of State (EOS-80). The
159 CTD salinity measurements were all standardized with International Association for
160 Physical Science of the Oceans (IAPSO) Standard Seawater (SSW) using the 1978
161 Practical Salinity Scale (PSS-78). We consider only data with good quality flags and
162 remove any obvious spikes in salinity data

163 We apply known salinity offsets owing to the different IAPSO SSW batches
164 used on the different cruise legs to the salinity data (Table A1). Batch-to-batch
165 offsets are from Kawano et al. (2006) and T. Kawano (personal communication

2011). They range from -1.2×10^{-3} to 2.5×10^{-3} PSS-78 (Table A1). SSW offsets could not be applied to 13 of the 73 Southern Ocean cruise legs analyzed here owing to 8 legs having no SSW batch number information available and 5 cruises using SSW batches too recent to have an offset estimate.

Additional ad-hoc salinity adjustments are estimated and applied to the CTD salinity data to further minimize intercruise measurement biases (Appendix A, Table A1, Figure A1). These salinity offsets are calculated by comparing salinity data in select geographical regions containing water that has been isolated from the surface for a relatively long time and is hence well-mixed with a very tight (low variance) θ-S relation (Appendix A). These additional offsets are necessary because of the relatively large contribution of salinity to density and the relatively high ratio of measurement error to signal observed here (Appendix A).

The ad-hoc salinity offsets are applied to 67 of the 73 Southern Ocean legs with magnitudes ranging from essentially zero ($< 10^{-6}$ PSS-78) to as high as 0.0056, with 63 of the applied offsets being less than the WOCE target accuracy of 0.002 (Fig. A1). The four legs with offset magnitudes > 0.002 PSS-78 are the 1984 occupation of P16, the 1993 and 1995 occupations of S03, and the 2011 occupation of A16 (Fig. A1; Table A1). A salinity offset could not be applied to six legs. These legs include the three occupations of S01 through the Drake Passage (Fig. 1) where highly variable water properties did not allow a suitable place for intercruise comparisons. Also three subsections of full lines are not long enough for salinity comparisons, namely the 1995, 2006, and 1991 occupations of I09, P18, and S03,

188 respectively. The salinity offsets are applied to the raw CTD salinity data and each
189 section occupation is re-gridded vertically and horizontally (P&J 2010).
190
191 **3. Methods: Heave vs. Water Property Changes**
192 Interior ocean property changes can be caused by heave or water-mass
193 changes (e.g., Fig. 2). A number of methods have been deployed for distinguishing
194 between heave and water-mass changes. For example, Bindoff and McDougall
195 (1994) decompose ocean property changes using S and θ changes on both density
196 and pressure surfaces and the original θ-S curve to solve for the contributions of
197 isopycnal heave, freshening, and salinification, whereas McDonagh et al. (2005)
198 calculate water-mass changes by calculating the "minimum distance" between
199 chronological θ-S curves, scaling them by thermal expansion and haline contraction
200 coefficients.
201 Here we use θ as the independent variable instead of density to allow
202 detection of very small deep θ-S changes. We make this choice because S errors
203 have significantly more impact on density than θ errors, especially in cold deep
204 waters. For example, at 4000 m in the Ross Sea, the expected measurement salinity
205 error of 0.002 PSS-78 will cause an error in density fifteen times larger than the
206 expected temperature error of 0.001 °C would cause. Therefore we choose the most
207 accurate measurement, θ, to be the independent variable in our analysis, rather than
208 density, which would amplify any remaining S errors.
209 As a result of this choice, here heave refers to a vertical shift of the water
210 column caused by a change in depth (equivalently pressure) of a potential isotherm

211 that has no effect on the local θ-S relationship (Fig. 2b). Alternatively, a water-mass
212 change is reflected in a shift in the shape of the θ-S curve with time (e.g. Fig. 2a).
213 While this method clearly identifies where θ-S changes occur, it casts all the water-
214 mass changes in terms of salinification (or freshening) and all warming (or cooling)
215 as owing to heave. For example, imagine a scenario in the deep Southern Ocean
216 (where θ decreases and S increases with increasing depth) where the whole water
217 column warms, causing the θ-S curve to be displaced upwards. Our analysis would
218 cast this water-mass change as freshening, with a value proportional to the warming
219 by the local slope of the θ-S curve. While deep AABW freshening presented here is
220 traced back to the shelf water changes that are freshening faster than warming (e.g.,
221 Jacobs and Guilivi 2010), the limitations of our method should be kept in mind.
222 To decompose the deep property changes, first we define an initial θ-S
223 relation (θ-S_i) representative of the θ-S at the time of the first occupation at every
224 location along a section. Each vertical profile of S and θ of each section is linearly
225 interpolated onto an evenly spaced θ grid from -2 to 5 °C at 0.01 °C intervals. The
226 interpolation extends from the bottom to the first θ maximum (usually the CDW θ-
227 maximum). All values above the maximum are masked out. The bottom S value of
228 each interpolated S profile is extended to the minimum bottom θ measured at that
229 location among all occupations of the section by using the slope of the linear fit of S
230 vs. θ over the coldest 0.1 °C of each profile. This extension is only applied if the
231 bottom $\theta < 3$ °C, the profile depth > 500 m, and the bottom 0.1 °C spans more than
232 100 m of the water column. These criteria limit extensions to deeper offshore
233 regions, excluding thermocline or continental shelf waters. Finally, S_i at each θ-grid

234 is estimated for the time of the first occupation from linear fits of S vs. time for all
235 occupations. If there are only two occupations, then S_i matches S of the first
236 occupation, but if there are multiple occupations of a section, then S_i will differ from
237 S of the first occupation.

238 The θ-S_i relations are used to calculate expected S values, S_H, if heave were
239 the only contributor to the changes in S. At each vertical and horizontal gridpoint
240 for each occupation, an S_H is computed from θ using a spline interpolant and the
241 local θ-S_i relation.

242 Finally, we calculate S rates of change for the total (S_T), S_H, and water-mass
243 shift (S_{WM}) with time and associated error as follows. At every horizontal and
244 vertical grid point along each section with at least two occupations spanning more
245 than 2.5 years (following P&J 2010) the rate of change of total S with time (dS_T/dt)
246 and dS_H/dt are estimated by linear least-squares (e.g. Fig. 3). Within the Southern
247 Ocean below 300 m, the trend error along sections with more than two occupations
248 is usually less than 0.4×10^{-3} PSS-78 yr^{-1}, smaller than most of the along-section
249 signal (e.g. Fig. 3). The rate of change in salinity with time owing to water–mass
250 shifts, $dS_{WM}/dt = dS_T/dt - dS_H/dt$, is calculated along each section (e.g. Fig.
251 3a,d,g,j,m). In addition, the rate of change of θ with time ($d\theta/dt$) is found also using
252 a linear least-squares fit (not shown, see P&J 2010).

253 For each deep basin (following P&J 2012; Fig. 1), the rates along all sections
254 within a given basin are used to find basin-mean rates and associated errors within
255 0.05 °C-thick bins below 5 °C. Along each section within a basin, using the mean θ
256 from all occupations, a θ-bin is identified as the region where θ falls within ±0.025

of a given value. Within each θ-bin area, first the vertical mean $d\theta/dt$, dS_T/dt, dS_{WM}/dt, and dS_H/dt are calculated along the sections. The vertical length of the given θ-bin at each location along the section is used to find a horizontal length-weighted mean rate (hereafter basin mean rates) for each θ-bin using all sections within a basin as if they were lined up end-to-end. The horizontal variance along a θ-bin is much larger than the vertical variance within a θ-bin. Therefore, we calculate and use the horizontal standard deviation of the vertical mean rates along a given isotherm (hereafter, basin standard deviations) for the basin error analyses. The basin standard deviations are also calculated as if all sections within a basin were connected end-to-end, differing from the section length-weighted mean technique used in P&J (2010). In addition, the basin standard deviations are usually larger than the slope errors on the rates themselves. Slope errors are neglected in the final error analysis, since they cannot be determined for most sections. Finally the degrees of freedom (DOF) for each isotherm bin are calculated using the horizontal length of the θ-bin following P&J 2010 assuming a 163–km decorrelation length scale (P&J 2010). The 95% confidence intervals are found for each basin for each θ-bin assuming a Student's t-distribution (e.g. Fig. 4).

4. Results

Throughout the Southern Ocean, water colder than 0 °C in each of the deep basins is freshening owing to water-mass changes, albeit in varying amounts, and becoming saltier below the CDW S-maximum owing to heave. The net effect is a deep freshening in the Indian and Pacific below 0°C with salinification above (Fig.

280 3a–l; Fig. 4b-c). In the South Atlantic, heave dominates to effect a full water column
281 salinification (Fig. 3m–o; Fig. 4a).

282 In the South Pacific, water-mass freshening dominates the total S signal in
283 waters below 0 °C throughout the Ross Gyre (west of 140ºW; Fig 3a,b,c), with
284 freshening increasing by an order of magnitude to 3 (±2) × 10^{-3} PSS-78 yr^{-1} in the
285 waters along the continental rise on the western side of the basin where the purest
286 and most recently formed RSBW flows westward (Jacobs and Giuivi 2010). This
287 strongest freshening along the continental rise in the coldest waters (θ < -0.4 ºC) is
288 almost completely owing to water-mass shifts (Fig. 4f), and is consistent with the
289 total freshening reported by Swift and Orsi (2012) in this region.. Within the
290 interior of the Ross Gyre, water-mass freshening is ~0.2 × 10^{-3} PSS-78 yr^{-1} for θ < 0
291 °C (Fig. 3a; Fig. 4c). The heave component causes an ~0.03 × 10^{-3} PSS-78 yr^{-1}
292 salinification between the bottom and 1000 m (Fig. 3b; Fig. 4c) owing to a reduction
293 in the volume of the coldest bottom waters, significantly different from zero at 95%
294 confidence in the basin mean for 0.2 < θ < 0.9 °C. These two counteracting factors
295 combine such that water-mass freshening dominates for θ < 0 °C, with a net
296 freshening of 0.16 × 10^{-3} PSS-78 $decade^{-1}$, while heave dominates between 0°C and
297 1000 m causing a net salinification (Fig. 3c; Fig. 4c;f). The Amundsen Basin (east of
298 140ºW) exhibits a slight water-mass freshening and heave salinification for zero net
299 change in salinity along S4P (Figs. 3a–c) and in the two meridional sections that
300 cross the basin (Fig. 1; not shown).

301 In the South Indian, water-mass freshening is present throughout AABW (Fig
302 3d,g,j), strongest along the continental slope, where recently formed RSBW and

303 ADLW flow westward before flowing north, ventilating the deep Australian-
304 Antarctic Basin (Orsi et al. 1999). Consistent with previous studies (Aoki et al. 2005;
305 Rintoul 2007; Johnson et al. 2008; Jacobs and Giuivi 2010; Shimada et al. 2012), our
306 results show a strong water-mass freshening, with basin-mean rates ranging from
307 1.2 (±0.6) × 10^{-3} PSS-78 yr^{-1} within the coldest (θ ~ -0.5 °C) bottom water to 0.2
308 (±0.1) × 10^{-3} PSS-78 yr^{-1} at θ = 0 °C (Fig. 4b,e). The freshening signal in the bottom
309 waters (θ < -0.2 °C) becomes gradually fainter from west to east: starting at ~0.6 ×
310 10^{-3} PSS-78 yr^{-1} in S03 (Fig. 3d, ~140ºE), to ~0.5 × 10^{-3} PSS-78 yr^{-1} in I09 (Fig. 3g,
311 ~115ºE), to ~0.3 × 10^{-3} PSS-78 yr^{-1} in I08 (Fig. 3j, ~90ºE). Again, heave partially
312 counteracts this freshening in all sections (Fig. 3e,h,k). The basin mean dS_H/dt
313 accounts for ~0.15 × 10^{-3} PSS-78 yr^{-1} of salinification, statistically significantly
314 different from zero for -0.3 < θ < 0.5 °C (Fig. 4b,e). The basin-mean dS/dt shows a
315 net freshening for θ < 0 °C and mostly a net salinification for θ > 0 °C (Fig. 3f,i,l; Fig.
316 4b,e).

317 In the South Atlantic, less water-mass freshening is observed with more
318 heave salinification, causing a very slight, and statistically insignificant net
319 salinification of ~0.1 (±0.13) × 10^{-3} PSS-78 yr^{-1} throughout the deep waters (θ < 0.4
320 °C; e.g. Fig.3 m,n,o; Fig. 4a,d). The zonal SR04 section across the Weddell Gyre
321 exhibits the most consistent trend among the sections crossing the Weddell-
322 Enderby Basin with a water-mass freshening of ~0.05 × 10^{-3} PSS-78 yr^{-1} in the
323 interior and slightly higher values along its east and west flanks, where the deep
324 westward flow of the southern limb of the Weddell Gyre and the northward-flowing
325 current carrying recently formed WSBW are found, respectively (Gordon et al.

2010). The heave, however, causes a bottom intensified salinification of ~0.1–0.3 × 10^{-3} PSS-78 yr^{-1} throughout much of the water column, consistent with a decrease in the volume of WSBW in the basin (P&J 2012), resulting in a net salinification across most of the section (Fig 3o). Section A12 (0 °E; not shown), which cuts meridionally through eastern end of the Weddell Gyre, is noisier than SR04, but roughly consistent within errors with the pattern seen along SR04. Further to the east, Section I06 (30ºE) across the Enderby Basin shows water-mass freshening of less than 0.1 × 10^{-3} PSS-78 yr^{-1}, smaller than the measurement error, but again consistent with other lines in this basin, along with a compensating heave of ~0.2 × 10^{-3} PSS-78 yr^{-1} (not shown). Together, these three lines yield a basin-mean salinification of 0.1 × 10^{-3} PSS-78 yr^{-1}, significantly different from zero at 95% confidence for $-0.2 < \theta < 0.5$ °C (Fig. 4a).

North of the Weddell-Enderby Basin, the Scotia Sea and the Argentine Basin, both fed by AABW from the Weddell Sea and vicinity (Fig. 1), show little bottom water salinity change rising above the noise. SR01 across Drake Passage (not shown) is extremely noisy and we can find no discernable signal. All sections crossing the Argentine Basin shows little water-mass change but a slight salinification owing to deep isotherm heave (not shown).

Finally, the basin-mean $d\theta/dt$ for all three of the southernmost basins exhibits statistically significant warming trends ranging from 0.002–0.005 °C yr^{-1} for $\theta < 0.5$ °C (Fig.4g-i). This trend is comparable to the 0.003 °C yr^{-1} warming P&J (2010) found below 3000 m south of the SAF, only here we have averaged along depths of mean potential isotherms within each basin instead of on isobaths as done

in P&J (2010). The basin-mean dθ/dt is more consistent along depth of mean isotherms (Fig. 4g–I vs. P&J (2010) Fig. 9d), arguably making this new calculation the preferable method.

5. Freshwater, heat and SLR budgets

Here we apply the basin means (Fig. 4) for water-mass, heave, total S, and θ trends over the entire Southern Ocean, here defined as south of 30°S, to evaluate their contributions to ocean freshwater budgets (Section 5a), global heat budgets (Section 5b), and SLR (Section 5c). For basins and the entire domain, the budget calculations are conducted from the bottom to three upper bounds: climatological θ = 0 °C as a rough proxy for the upper boundary of AABW (Foster and Carmack, 1976), 4000 m for a deep ocean estimate where water properties are most strongly influenced by AABW (Johnson 2008; following P&J 2010), and 2000 m to extended our analysis to the current maximum sampling depth of Argo floats (e.g. Roemmich et al. 2009).

The basin-mean rates and errors are applied to the climatological θ and S fields (Gouretski and Koltermann 2004). The climatological θ and S vertical profiles are put onto a uniform 20-m depth grid using a shape-preserving piecewise cubic interpolation. Each basin-mean rate and its standard deviation on the θ-grid (Fig. 4) are interpolated onto the climatological θ profiles at each horizontal gridpoint, assigning all four rates and their standard deviations as discussed above. Regions above the CDW θ maximum are not considered here since the method used does not allow it. Given the focus on AABW changes, this limitation is minor.

372

373 *a. Freshwater budget*:

374 Here we quantify the fresh water uptake owing to deep water-mass changes
375 in the deep Southern Ocean, including in AABW, and compare its magnitude to that
376 of the excess mass flux off Antarctica in recent decades from ice melt. We estimate
377 the freshwater flux by calculating the amount of freshwater (V_{fw}) necessary to add
378 to an initial volume (V_i) with initial salinity (S_i) in order to cause the water to
379 freshen at the observed dS_{WM}/dt over a 1-year period to a final salinity (S_f). If salt is
380 conserved and we only change the salinity by adding freshwater to the system to
381 change V_i to a final volume (V_f), then V_{fw} is calculated as:

382 $$V_{fw} = \int V_f - V_i = \int \left(\frac{S_i}{S_f} - 1 \right) \cdot dv, \quad (1)$$

383 neglecting the relatively small change in density. Here S_i is the gridded
384 climatological salinity (Gouretski and Koltermann 2004) and S_f is calculated by
385 applying dS_{WM}/dt for one year at each climatological grid point. The *dv* for each grid
386 point is calculated as the volume of the half-degree longitude by a half-degree
387 latitude by 20-m depth box. Local freshwater fluxes in m yr^{-1} are found by
388 integrating in the vertical from the bottom to θ = 0 ºC, 4000 m, and 2000 m (Fig 5)
389 and basin totals by integrating over the whole basin below the same surfaces (Table
390 1). The standard deviations of V_{fw} for the basin means are found by applying S_f ±
391 one standard deviation of S_f in (1). The basin DOFs are θ volume-weighted mean
392 along-isotherm DOFs below a given surface (Fig. 4) and the 95% confidence interval
393 is calculated using a Student's t-distribution (Table 1). Finally, a total for the whole

394 Southern Ocean below each top surface is calculated as a sum of all the basin values
395 south of 30 °S with 95% confidence intervals found using the sum of the basin
396 standard deviations and DOFs (Table 1).

397 Local estimates from the bottom to θ = 0 ºC show the largest deep
398 freshening occurring in the west Pacific and Indian Ocean sectors (Fig. 5). The local
399 freshwater flux in these regions for θ = 0 ºC exceeds 0.02 m yr^{-1} over the north-west
400 corner of the Amundsen–Bellingshausen Basin and most of the deep portions of the
401 Australian-Antactic Basin (Fig. 5a), despite θ < 0 ºC occupying only ~1000–1500 m
402 of the water column. This flux is equivalent to a total freshwater addition of 25 ±9
403 and 48 ±36 Gt yr^{-1} into the Amundsen-Bellingshausen and Australian-Antarctic
404 basins, respectively (Table 1), suggesting that a large fraction of the estimated
405 recent 140 Gt yr^{-1} freshwater flux from ice melt (Rignot et al. 2008) may be taken up
406 by freshening AABW.

407 The Weddell-Enderby Basin also shows a slight freshwater flux of 0.005 m yr^{-1}
408 below θ = 0 °C (Fig.5). This small amount reflects the very slight observed 0.1×10^{-3}
409 PSS-78 yr^{-1} water-mass freshening (Fig. 4a) applied to the relatively large volume
410 of AABW, with water of $\theta \leq 0$ °C isotherm as much as 4000 m in thickness (e.g. Fig.
411 3m). The relatively large volume of AABW combined with the small water-mass
412 freshening, gives an rather uncertain total freshening of 24 ±54 Gt yr^{-1}.

413 Integrating vertically to 4000 and 2000 m, further emphasizes the pattern
414 discussed above south of the SAF and shows a strong water-mass salinification in
415 the NADWs north of the SAF at intermediate depths (Fig. 5, Table 1). Integrating to
416 4000 m, containing only a fraction of θ < 0 °C (Fig. 3; bold black contours), gives a

fraction the freshening seen for θ < 0 °C (Fig. 5b). Integrating to 2000m (Fig. 5c), the local water-mass freshwater flux south of the SAF is almost identical as that from integrating to the 0 °C isotherm, indicating that water-mass freshwater changes are mostly constrained to θ < 0 °C with little water-mass freshening in the waters between 0 °C and 2000m (Fig. 3a,d,g,j). South of the SAF 2000 m lies below CDW entering from the north, therefore, none of these isotherms or isobar surfaces reflect changes in CDW south of the SAF. However, north of the SAF between 2000 and 3000 m, in the waters heavily influenced by NADW with θ ~ 2.8 °C, a strong salinification is observed, seen as a negative local fresh water fluxes of between -0.01 and -0.1 m yr^{-1} in the local fluxes (Fig 5c). These waters are also freshening and warming from heave (not shown). The property changes in these regions are separate from the deep AABW changes discussed in this paper, and likely indicate physical changes in the NADW in these regions.

b. Heat budget

We find large and statistically significant heat uptake in each basin and the whole Southern Ocean for θ < 0°C, below 4000 m, and below 2000 m (Table 1). The rate of heat gain (Q) is given by

$$Q = \int \rho \cdot C_p \cdot {}^{d\theta}\!/_{dt} \cdot dv, \tag{2}$$

where density (ρ) and heat capacity (C_p) are calculated from the climatological θ, S, and pressure at each grid point. The standard deviation of Q is found by replacing dθ/dt in (2) with the standard deviations of dθ/dt. We sum the errors because the

439 individual grid points are not independent of each other. The total DOF and 95%
440 confidence intervals for each basin and total Southern Ocean (Table 1) are
441 estimated by previously described methods (Section 5a). We find a large,
442 statistically significant, heat gain thoughout the water column in the Southern
443 Ocean. Totals found here are slightly smaller, but within the error, of P&J (2010;
444 discussed further is section 6).
445
446 *c. Sea Level Rise*
447 Changes in density of AABW owing to dS_T/dt, dS_{WM}/dt, dS_H/dt and $d\theta/dt$
448 contribute to halosteric and thermosteric SLR. We calculate the contribution of each
449 component to SLR using:

450 $$SLR_{halostaric} = \frac{\int -\beta \cdot dS/dt \cdot dv}{SA} \text{ and } SLR_{\theta} = \frac{\int \alpha \cdot d\theta/dt \cdot dv}{SA}, \quad (3)$$

451 where the thermal expansion coefficient, α, and the haline contraction coefficient, β,
452 are calculated locally from the climatological gridded θ, S, and pressure. For a local
453 estimate, the integral is evaluated vertically from the bottom to a top surface at each
454 grid point where the surface area (SA) has the surface area of that grid point,
455 yielding its contribution to local SLR in mm yr^{-1} (Fig. 6). Again, the top surfaces
456 considered here are θ = 0 °C, 4000 m, and 2000 m. For each basin an average SLR is
457 calculated using (3) where the volume integral is now over the entire region from
458 the bottom to the top surface under consideration, and SA is the surface area of that
459 top surface for the basin (Table 1). The gridded standard deviations are integrated
460 again using (3) to estimate the total basin standard deviation. The 95% confidence

intervals are estimated assuming Student's t-distribution and using the total DOF below a given surface as described in Section 5a.

Water-mass freshening tends to reduce SLR in all three southernmost basins while the heave salinification raises SLR (Fig. 6). The local effects of water-mass freshening vary spatially, but follow the spatial patterns seen in the freshwater flux (Fig. 5), with the strongest signal seen in the South Pacific and South Indian (Fig 6a,e,i). Heave salinification counteracts some of the SLR, except in the Amundsen-Bellingshausen Basin (Fig. 6b,f,j; Table 1). The net effect is a slight (~-0.02 mm yr^{-1}) local negative SLR in the South Atlantic and a net positive (~0.03 mm yr^{-1}) SLR in the South Pacific and South Indian sectors of the Southern Ocean (Fig. 6c,g,k; Table 1). The salinity contribution, however, is still smaller than the warming contribution of 1–2 mm yr^{-1} throughout the Southern Ocean (Fig. 6d,h,l).

6. Discussion

The Southern Hemisphere has experienced dramatic changes in recent decades owing to increases in atmospheric concentration of greenhouse gases and ozone–depleting chemicals. These changes include increased Southern Ocean warming (Gille 2008), increased glacial melt in the East Antarctic and Antarctic Peninsula (Rignot et al. 2008), a global slowdown of the bottom limb of the MOC (Kawano et al. 2010, Kouketsu et al. 2011; P&J 2012), and freshening of AABW (Jacobs and Guilivi 2010, Swift and Orsi 2012). Here we have examined property changes in the deep Southern Ocean, distinguishing between changes in the θ–S relation and vertical heave of θ surfaces within and associated with AABW. We

484 conclude with a discussion comparing the amount of warming and freshening
485 estimated in AABW to the global radiative imbalance, total glacial meltwater runoff
486 from Antarctica, and global mean SLR.

487 Freshening of AABW in the Pacific and Indian sectors of the deep Southern
488 Ocean appears to accounts for roughly half of the net Antarctic continental ice melt
489 of recent years. The strongest freshening owing to water-mass shifts is seen near
490 the AABW source regions and follows the path of AABW deep circulation in the
491 three southernmost basins (Fig. 5a) reflecting the advection of a fresher variety of
492 AABW into the deep Southern Ocean. The strongest freshening signal in the
493 youngest AABW waters to the south with no freshening observed in the older AABW
494 further to the north (Fig. 5) suggests that this freshening flux may have started
495 relatively recently. The Amundsen coast freshwater flux into the South Pacific and
496 South Indian oceans that freshens the shelf water components of AABW there is
497 probably largely owing to net continental ice melt (Jacobs and Guilivi 2010),
498 estimated to be 140 Gt yr^{-1} over recent decades (Rignot et al. 2008). Our estimates
499 are that the deep Amundsen-Bellingshausen and Australian-Antarctic basins have
500 exhibited increases of 25 ±9 and 48 ±36 Gt $yr^{-1,}$ respectively, of fresh water between
501 roughly 1991 and 2008, making the deep ocean a significant sink for the recent
502 increase in glacial melt. The Weddell Basin also exhibits hints of water-mass
503 freshening, albeit at a slower rate that is smaller than the measurement error.
504 However, the spatial pattern of strongest freshening in the newest AABW and the
505 consistency of the freshening throughout the basin (Fig. 3m) suggest that Weddell
506 AABW may also be getting fresher.

507 The heave component of AABW changes found here reflects a loss of volume
508 in AABW over time, seen farther from the source than the advected water mass
509 freshening signal because production rate changes are communicated by pressure
510 waves on much shorter time scales (e.g., Masuda et al. 2010). P&J (2012) found an 8
511 SV loss in volume of deep Southern Ocean water colder than 0°C, suggesting a recent
512 decrease in the production of AABW. Paleoproxies indicate that the bottom limb of
513 the MOC has been in multiple steady states during different climate regimes (Lynch-
514 Stieglitz et al. 2007). Current water-mass volumes and chemistry of the global
515 inventory of AABW vs. NADW suggest that past rates of AABW production may have
516 been higher, also supporting the hypothesis of smaller production rates of AABW in
517 recent decades (Broecker et al. 1999; Johnson 2008). Here we separate heave from
518 water-mass changes in the deep ocean and show that while the water-mass changes
519 are currently limited to the deep basins adjacent to Antarctica, heave is responsible
520 for part of the deep ocean changes there, and most, if not all, of the deep ocean
521 changes in AABW further north. Furthermore, the deep volume loss of water colder
522 than 0 °C is consistent with the warming and salinification of the water between 0 °C
523 isotherm and 1000 m in the South Indian and South Pacific oceans (Fig. 3b,e,h,k,n).
524 AABW warming from heave contributes to the net ocean heat uptake. Earth
525 is currently out of radiative balance owing to increasing atmospheric greenhouse
526 gas concentrations. Satellite and in situ measurements show that Earth has been
527 gaining heat at a rate of 183 TW between 1972 and 2008 (Church et al. 2011) with
528 90% of the excess energy being absorbed by the ocean. For comparison, the 33.8
529 ±3.1 TW of warming found here south of 30ºS below 2000 m (Table 1) amounts to

about 0.07 ±0.01 W m^{-2} when calculated as a flux over the entire Earth surface. This is about 14% of the above total heat uptake.

The values of heat gain we find in the Southern Ocean are generally smaller than those of P&J (2010), and have smaller confidence intervals. Our mean heat fluxes below 4000 m in the Amundsen-Bellingshausen, Australian-Antarctic, and Weddell-Enderby basins are 0.14 ±0.05, 0.11 ±0.07, and 0.23 ±0.10 W m^{-2}, respectively. Comparable values from P&J (2010) are 0.20 ±0.14, 0.32 ±0.17, and 0.44 ±0.36 W m^{-2}, respectively. These two sets of estimates agree within confidence limits. While some data have been added for the most recent estimates, much of the difference is owing to a change in methods. We now find basin means on mean θ depths and apply them by θ to the climatological mean θ field instead of doing calculations on isobars. This new method gives smaller heat gains than P&J (2010) because the large warming in the deep southernmost waters raises the whole basin mean along an isobar, thus raising the basin total when integrated on isobars. When the rates are calculated and applied on θ, the strongest signal in contained geographically to the deep southernmost region, thus giving a more accurate, but smaller total heat flux. The 95% confidence intervals are slightly smaller here than in P&J (2010) partly because we use more data, but mostly because the variations across the basin are smaller on mean depths of isotherms than along isobars.

Finally, both the observed heave and water-mass freshening signals in the deep Southern Ocean contribute to SLR (Table 1). Global mean sea level is estimated to rise at a rate of 3.1 mm yr^{-1} between 1993 and 2003, with 1.6 ±0.5 mm yr^{-1} owing to thermal expansion in the upper water column and the rest owing to ice melt

553 (Bindoff et al. 2007). Water property changes south of 30ºS for $\theta < 0$ °C cause a local
554 mean SRL or 0.52 ±0.18 mm yr^{-1} with almost all of this owing to changes in θ (Table
555 1). The heave component accounts for a positive SLR of 0.44 mm yr^{-1}, with 0.52
556 ±0.17 mm yr^{-1} owing to warming and a negative 0.08 ±0.04 SLR from salinification.
557 The water-mass freshening causes an additional 0.09 ±0.05 mm yr^{-1}. Therefore, in
558 the deep Southern Ocean, local SLR owing to AABW changes are a significant
559 fraction of the global mean rate of SLR.
560
561 *Acknowledgments:*
562 We thank the hundreds of people who helped to collect, calibrate, process,
563 and archive the WOCE and CLIVAR data sets, without whom global assessments of
564 ocean variability like this one would be impossible. We also thank those who
565 provided us with unreported SSW batch numbers for many cruises. D. Roemmich
566 suggested an improvement for the error analysis. This work was supported by the
567 NOAA Climate Program Office, NOAA Research, and NASA Headquarters under the
568 NASA Earth and Space Fellowship Program - Grant NNX11AL89H.
569
570

APPENDIX

Ad-hoc Salinity Adjustments

We attempt to correct for small intercruise salinity biases as offsets for all occupations of repeated hydrographic sections (Table A1; see P&J 2012 for full data set description). We estimate these offsets by comparing S data in select geographical regions containing old, well-mixed, low-variability water, where old refers signifies a long time since the water was last in contact with the atmosphere. These small intercruise S biases can arise from differences in sampling, measuring, and calibration routines conducted by different personnel.

Intercruise S offsets are identified for all occupations of every section. First, each cruise is divided into subsections based on topographic and dynamic boundaries (such as fronts). Areas near boundaries, strong currents, or water-mass fronts are excluded. For each occupation at each location along a section, the S data are linearly interpolated onto to a 0.01 °C resolution θ-grid. The intercruise difference in S, ΔS, is calculated at each θ and each location along the section by subtracting the mean S of all the co-located occupations from each individual occupation. A mean (ΔS_{mean}) and variance (ΔS_{var}) are calculated for each subsection along θ surfaces. Within each subsection, a 0.1 °C-thick layer is chosen balancing where ΔS_{var} is small and the waters are oldest, as determined by examination of the chlorofluorocabon, oxygen, nitrate, and $\Delta^{14}C$ distributions for the WOCE occupation of each section using the WOCE Atlases (e.g., Orsi and Whitworth, 2005). These portions of the water column are chosen to maximize the likelihood that ΔS

593 estimates are owing to cruise measurement biases, not physical changes. The
594 weighted means of ΔS_{mean}, $\Delta \overline{S}_{mean}$, within the selected isotherm bands are found
595 using the inverses of ΔS_{var} for weights. Similarly, the weighted means of ΔS_{var} , $\Delta \overline{S}$
596 $_{var,}$ are found using ΔS_{var} as weights. Finally, the S offset for an entire cruise is
597 calculated as the $\Delta \overline{S}_{var}$ weighted mean of $\Delta \overline{S}_{mean}$ (Table A1).

598 The global array of repeated hydrographic sections collected through WOCE
599 and GOSHIP programs are considered here, consisting of 33 lines with a total of 146
600 legs collected between 1981 and 2012. SSW batches and their recommended SSW
601 offsets (Kawano et al. 2006; T. Kawano personal comm. 2011) are noted along with
602 the additional ad-hoc offset found here (Table A1). Offsets are added to salinity data
603 to obtain the final value. SSW batch offsets are available for 91% of the legs, with
604 missing values either because the SSW batch used is too new for an offset to be
605 estimated or because the SSW batch used is unknown. Additional ad-hoc offsets are
606 found for 87% of the legs, with the missing offsets owing to the leg length being too
607 short or the absence of a location on the section suitable to identify an offset. Of the
608 132 net offsets, 118 are less than the stated CTD salinity accuracy of 0.002 PSS-78,
609 with the mean magnitude of the offsets being 0.0008 PSS-78 (Fig A1). While the
610 application of SSW batch offsets improves the agreement among occupations of each
611 section, it does not eliminate the need for ad-hoc offsets to reduce intercruise
612 salinity biases (Fig. A1).

613 While these offsets are small, they are important for sea level rise estimates.
614 For example, a 0.002 PSS-78 increase in S applied a 1000-m of a 0°C, 34.6 PSS-78
615 column of water results in a 0.14 mm decrease in SLR compared to only a 0.03 mm

SLR increase from a 0.002 °C increase in temperature. In addition, the observed freshening between sequential cruises ~10 years apart, ranges from 0 to 1 order of magnitude greater than the WOCE stated salinity accuracy but 1 to 2 orders of magnitude greater than the WOCE temperature accuracy.

620 References

621 Aoki, S., S. R. Rintoul, S. Ushio, S. Watanabe, and N. L. Bindoff, 2005: Freshening of
622 the Adélie Land Bottom Water near 140°E. *Geophys. Res. Lett.,* **32**, L23601,
623 doi:10.1029/2005GL024246.
624 Church, J. A.., N. J. White, L. F. Konikow, C. M. Domingues, J. G. Cogley, E. Rignot, J. M.
625 Gregory, M. R. van den Broeke, A. J. Monaghan, and I. Velicogna, 2011: Revisiting
626 the Earth's sea-level and energy budgets from 1961 to 2008. *Geophys. Res. Lett.,*
627 **38,** L18601, doi:10.1029/2001GL048794.
628 Coles, V. J., M. S. McCartney, D. B. Olson, and W. M. Smethie Jr., 1996: Changes in
629 Antarctic Bottom Water properties in the western South Atlantic in the late
630 1980s. *J. Geophys. Res*., **101**, 8957–8970.
631 Bindoff, N.L., and T.J. McDougall, 1994: Diagnosing Climate Change and Ocean
632 Ventilation using Hydrographic Data. Journal of Physical Oceanography, **24**,
633 1137-1152. ISSN 1520-0485.
634 Bindoff, N. L., J. Willebrand, V. Artale, A, Cazenave, J. Gregory, S. Gulev, K. Hanawa, C.
635 Le Quéré, S. Levitus, Y. Nojiri, C. K. Shum, L. D. Talley, and A. Unnikrishnan, 2007:
636 Observations: Oceanic Climate Change and Sea Level. In: *Climate Change 2007:*
637 *The Physical Science Basis. Contribution of Working Group I to the Fourth*
638 *Assessment Report of the Intergovernmental Panel on Climate Change* [Solomon,
639 S., D. Qin, M. Manning, Z. Chen, M. Marquis, K.B. Averyt, M. Tignor and H.L. Miller
640 (eds.)]. Cambridge University Press, Cambridge, United Kingdom and New York,
641 NY, USA.

642 Broecker, W. S., S. Sutherland, and T. H. Peng, 1999: A possible 20th-century
643 slowdown of Southern Ocean deep water formation. *Science* **286**, 1132-1135,
644 doi:10.1126/science.286.5442.1132.
645 Fahrbach, E., M. Hoppema, G. Rohardt, M. Schroder, and A. Wisotzki, 2004: Decadal-
646 scale variations of water mass properties in the deep Weddell Sea. *Ocean*
647 *Dynamics*, **54**, 77–91.
648 Fahrbach E., M. Hoppema, G. Rohardt, O. Boebel, O. Klatt, and A. Wisotzki, 2011:
649 Warming of deep and abyssal water masses along the Greenwich meridian on
650 decadal time scales: The Weddell gyre as a beat buffer. *Deep-Sea Res. II,* **58**,
651 2508–2523, doi:10.1016/j.dsr2.2011.06.007*.*
652 Foster, T. D., and Carmack, E. C., 1976: Frontal zone mixing and Antarctic Bottom
653 Water formation in the southern Weddell Sea. *Deep-Sea Res.*, **23**, 301–317.
654 Fukasawa, M., H. Freeland, R. Perkins, T. Watanabe, H. Uchida, and A. Nishima, 2004:
655 Bottom water warming in the North Pacific Ocean. *Nature*, **427**, 825–827.
656 Gille, S. T., 2008: Decadal-scale temperature trends in the Southern Hemisphere
657 ocean. *J. Climate*, **21**, 4749–4765.
658 Gordon, A. L., 1972: Spreading of Antarctic Bottom Waters, II In: *Studies in Physical*
659 *Oceanography - A Tribute to George Wust on His 80th Birthday*. A.L. Gordon (ed),
660 Gordon and Breach, Science Publ., N.Y.: 1-17.
661 Gordon A. L., B. Huber, D. McKee, and M. Visbeck, 2010; A Seasonal cycle in the
662 export of bottom water from the Weddell Sea. *Nature Geoscience*, **3**, 551-556,
663 doi:10.1038/ngeo916.

664 Gouretski, V. V., and K. P. Koltermann, 2004: *WOCE Global Hydrographic Climatology.*
665 Berichte des bundesamtes für seeshifffahrt und hydrographie, 35, pp. 52+2 CD-
666 ROMs.
667 Jacobs, S. S., 2004: Bottom water production and its links with the thermohaline
668 circulation. *Antarctic Science*., **4**,427-437, doi:10.1017/S095410200400224X.
669 Jacobs, S. S., and C. F. Giulivi, 2010: Large multi-decadal salinity trends near the
670 Pacific-Antarctic Continental Margin. *J. Climate*, **23**, 4508–4524,
671 doi:10.1175/2010JCLI3284.1.
672 Johnson, G. C., 2008: Quantifying Antarctic Bottom Water and North Atlantic Deep
673 Water volumes. *J. Geophys. Res*., **113**, C05027, doi:10.1029/2007JC004477.
674 Johnson, G. C., and S. C. Doney, 2006: Recent western South Atlantic bottom water
675 warming. *Geophys. Res. Lett*., **33**, L14614, doi:10.1029/2006GL026769.
676 Johnson, G. C., S. Mecking, B. M. Sloyan, and S. E. Wijffels, 2007: Recent bottom water
677 warming in the Pacific Ocean. *J. Climate*, **20**, 5365–5375.
678 Johnson, G. C., S. G. Purkey, and J. L. Bullister, 2008: Warming and freshening in the
679 abyssal southeastern Indian Ocean. *J. Climate*, **21**, 5353–5365.
680 Joyce, T. M., 1991: Introduction to the collection of expert reports compiled for the
681 WHP Program. WOCE Hydrographic operations and methods. WOCE Operations
682 Manual. WHP Office Report WHPO-91-1, WOCE Report 68/91.
683 Kawano, T., M. Aoyama, T. Joyce, H. Uchida, Y. Takatsuki, and M. Fukasawa, 2006:
684 The latest batch-to-batch difference table of standard seawater and its
685 application to the WOCE onetime sections. *J. Oceanogr.,* **62**, 777-792.

686 Kawano, T., T. Doi, H. Uchida, S. Kouketsu, M. Fukasawa, Y. Kawai, and K. Katsumata,
687 2010: Heat content change in the Pacific Ocean between the 1990s and 2000s.
688 *Deep-Sea Res. II,* **57**, 1141–1151, doi:10.1016/j.dsr2.2009.12.003.
689 Kouketsu, S., and Coauthors, 2011: Deep ocean heat content changes estimated from
690 observation and reanalysis product and their influence on sea level change. *J.*
691 *Geophys. Res.*, **116**, C03012, doi:10.1029/2010JC006464.
692 Lumpkin, R., and K. Speer, 2007, Global ocean meridional overturning. *J. Phys.*
693 *Oceanogr.,* **37**, 2550–2562.
694 Lynch-Stieglitz, J., and Coauthors, 2007: Atlantic meridional overturning circulation
695 during the last glacial maximum. *Science,* **316**, 66–69,
696 doi:10.1126/science.1137127.
697 Masuda, S., and Coauthors, 2010: Simulated rapid warming of abyssal North Pacific
698 water. *Science*, **329**, 319–322, doi:10.1126/science.1188703.
699 McDonagh E. L., H. L. Bryden, B. A. King, R. J. Sanders, S. A. Cunningham, and R.
700 Marsh, 2005: Decadal changes in the south Indian Ocean thermocline. *J. Climate*,
701 **18**, 1575-1590.
702 Meredith, M. P., A. C. Naveira Garabato, A. L. Gordon, and G. C. Johnson, 2008:
703 Evolution of the deep and bottom water of the Scotia Sea, Southern Ocean,
704 during 1995–2005. *J. Climate*, **21**, 3327–3343.
705 Orsi., A. H. , T. Whitworth II, Hydrographic Atlas of the World Ocean Circulation
706 Experiment (WOCE). Volume 1: Southern Ocean (eds. M. Sparrow. P. Chapman
707 and J. Gould), International WOCE Project Office, Southampton, U.K., ISBN 0
708 904175-49-9. 2005.

709 Orsi, A. H., G. C. Johnson, and J. L. Bullister, 1999: Circulation, mixing and production
710 of Antarctic Bottom Water. *Prog. Oceanogr.*, **43**, 55–109.
711 Purkey, S. G., and G. C. Johnson, 2010, Warming of global abyssal and deep Southern
712 Ocean waters between the 1990s and 2000s: Contributions to global heat and
713 sea level rise budgets. *J. Climate*, **23**, 6336–6351. doi:10.1175/2010JCLI3682.1.
714 Purkey, S. G. and G. C. Johnson, 2012: Global contraction of Antarctic Bottom Water
715 between 1980s and 2000s. *J. Climate*, **25**, 5830–5844. doi:10.1175/JCLI-D-11-
716 00612.1
717 Rignot, E., J. L. Bamber, M. R. van Den Broeke, C. Davis, Y. Li, W. Jan Van De Berg, and
718 E. van Meijgaard, 2008: Recent Antarctic ice mass loss from radar interferometry
719 and regional climate modeling. *Nature Geoscience*, **1,** 106–110,
720 doi:10.1038/ngeo102.
721 Rignot E., and S. S. Jacobs, 2002: Rapid bottom melting widespread near Antarctic
722 ice sheet grounding lines. *Science*, **296**, 2020-2023,
723 doi:10.1126/science.1070942.
724 Rintoul, S. R., 2007: Rapid freshening of Antarctic Bottom Water formed in the
725 Indian and Pacific oceans. *Geophys. Res. Lett.*, **34**, L06606,
726 doi:10.1029/2006GL028550.
727 Robertson R., M. Visbeck, A. L. Gordon, and E. Fahrbach, 2002: Long-term
728 temperature trends in the deep waters of the Weddell Sea. *Deep-Sea Res. II*, **49**,
729 4791–4806.

730 Roemmich, D., G. C. Johnson, S. Riser, R. Davis, J. Gilson, W. B. Owens, S. L. Garzoli, C.
731 Schmid, and M. Ignaszewski. 2009. The Argo Program: Observing the global
732 oceans with profiling floats. *Oceanography*, **22(2)**, 34-43.
733 Shepherd, A., D. J. Wingham, and J. A. D. Mansley, 2002: Inland thinning of the
734 Amundsen Sea sector, West Antartica. *Geophys. Res. Lett*, **29**,
735 doi:10.1029/2001GL014183.
736 Shepherd, A., D. Wingham, and E. Rignot, 2004: Warm ocean is eroding West
737 Antarctic Ice Sheet. *Geophys. Res. Lett*, **31**, L23402, doi:10.1029/2004GL021106.
738 Shimada, K., S. Aoki, K. I. Ohshima, and S. R. Rintoul, 2012: Influence of Ross Sea
739 Bottom Water changes on the warming and freshening of the Antarctic Bottom
740 Water in the Australian-Antarctic Basin. *Ocean Sci.*, **8**, 419-432, doi: 10.5194/os-
741 8-419-2012.
742 Swift J. H., and A. H. Orsi, 2012: Sixty-four days of hydrography and storms: RVIB
743 Nathaniel B. Palmer's 2011 S04P Cruise. *Oceanography*, **25(3)**, 54-55,
744 doi:10.5670/oceanog.2012.74.
745 Whitworth, T., III, 2002: Two modes of bottom water in the Australian-Antarctic
746 Basin, *Geophys. Res. Lett.*, **29**, 1073, doi:10.1029/2001GL014282.
747 Zenk, W., and E. Morozov, 2007: Decadal warming of the coldest Antarctic Bottom
748 Water flow through the Vema Channel. *Geophys. Res. Lett.*, **34**, L14607,
749 doi:10.1029/2007GJ030340.
750

750 Table 1: Fresh water gain (FW; Gt yr^{-1}), Sea Level Rise (SLR; mm yr^{-1}) and heat
751 uptake (TW) with uncertainties at the 95 % confidence level below θ = 0 °C, 4000 m,
752 and 2000m in the Amundsen-Bellingshausen Basin (ABB), Australian-Antarctic
753 Basin (AAB), Weddell-Enderby Basin (WEB) and the whole Southern Ocean south of
754 30°S (Fig. 1). Freshwater estimates are calculated following (1) using basin mean
755 freshening trends owing to only water-mass changes. The steric SLR is estimated
756 from (3) broken into water-mass, heave, total salinity, and warming trends. The
757 total steric SLR is also given. Heat uptake is calculated following (2) using basin
758 mean warming trends.
759

		FW (Gt yr^{-1})	SLR (mm yr^{-1})					Heat (TW
		Water-mass	Water-mass	Heave	Salinity	θ	Total	θ
Below 0 C	ABB	25 ±9	0.17 ±0.06	0.00 ±0.02	0.18 ±0.07	0.31 ±0.10	0.49 ±0.13	1.0 ±0.5
	AAB	48 ±36	0.22 ±0.16	-0.07 ±0.05	0.15 ±0.18	0.5 ±0.28	0.65 ±0.33	2.5 ±1.3
	WEB	24 ±54	0.05 ±0.11	-0.12 ±0.12	-0.07 ±0.12	0.66 ±0.45	0.59 ±0.46	7.7 ±2.8
	Total S of 30S	99 ±56	0.09 ±0.05	-0.08 ±0.04	0.00 ±0.06	0.52 ±0.17	0.52 ±0.18	14 ±3
Below 4000m	ABB	9 ±4	0.03 ±0.01	-0.01 ±0.01	0.02 ±0.02	0.18 ±0.06	0.20 ±0.06	1.1 ±0.4
	AAB	17 ±13	0.12 ±0.1	-0.02 ±0.03	0.11 ±0.1	0.14 ±0.13	0.25 ±0.17	0.4 ±0.2
	WEB	10 ±28	0.03 ±0.09	-0.05 ±0.08	-0.02 ±0.05	0.30 ±0.23	0.28 ±0.24	1.9 ±0.8
	Total S of 30S	53 ±21	0.02 ±0.01	-0.02 ±0.01	0.01 ±0.01	0.13 ±0.05	0.14 ±0.05	5 ±1
Below 2000m	ABB	-28 ±43	-0.05 ±0.08	0.02 ±0.07	-0.03 ±0.08	0.44 ±0.26	0.41 ±0.27	5.7 ±1.8
	AAB	48 ±66	0.15 ±0.2	-0.12 ±0.21	0.03 ±0.29	1.03 ±0.83	1.06 ±0.89	8.1 ±3.5
	WEB	27 ±81	0.06 ±0.17	-0.13 ±0.19	-0.07 ±0.2	0.70 ±0.70	0.63 ±0.73	7.8 ±2.9
	Total S of 30S	-454 ±241	-0.12 ±0.06	0.09 ±0.07	-0.03 ±0.06	0.37 ±0.15	0.34 ±0.16	34 ±3

760
761

761 Table A1: IAPSO Standard Sea Water (SSW) batch number with recommended SSW
762 batch salinity offset (Kawano et al. 2006; T. Kawano personal communication 2011)
763 for each leg (listed by year) of all sections (listed by WOCE ID; Fig. 1). If no SSW
764 batch number is listed, we were unable to determine this information from cruise
765 reports or through personal queries to data originators. As of September 2012,
766 there is no known offset for batch numbers P113 and P152, therefore no SSW batch
767 offset is applied for cruises using those SSW batches. The last column lists the
768 additional ad-hoc salinity offsets estimated by and applied for our analyses (see
769 Appendix). If legs do not have an ad-hoc salinity offset listed, then one was not
770 possible to estimate owing to the section location or length. Both offsets are added
771 to salinity data.

WOCE ID	Yr	SSW batch number	SSW offset (x1000)	ad-hoc offsets (x1000)
A01	1990	P112	1.9	0.186
A01	1990	P104	1.1	N/A
A01	1991	P112/P114	1.9/2	N/A
A01	1991	P112	1.9	-0.288
A01	1992	P119	0	-0.836
A01	1992	P112	1.9	N/A
A01	1994	N/A	N/A	N/A
A01	1994	P123	0.7	N/A
A01	1994	P124	0.6	-0.496
A01	1995	N/A	N/A	-0.551
A01	1995	P126	0.6	N/A
A01	1996	N/A	N/A	1.870
A01	1996	P124	0.6	N/A
A01	1997	P129	0.4	N/A
A01	1997	P129	0.4	N/A
A01	1993	P117	N/A	N/A
A01	1998	P133	0.3	N/A
A02	1994	P124	0.6	-1.849
A02	1997	P129	0.4	1.849
A05	1981	P93	0.9	-2.867
A05	1992	P120	-0.9	0.114
A05	1998	P125	0.2	0.259

A05	2004	P143/P144	-0.2/-0.5	1.028
A05	2010	N/A	N/A	1.952
A10	1992	P120	-0.9	-1.110
A10	2003	P142	0.2	0.134
A10	2011	P152	N/A	0.829
A12	1992	P114	2	-0.553
A12	1999	P134	0.3	-0.038
A12	2000	P135	0.2	0.624
A12	2002	P140	-0.3	-0.034
A12	2005	P144	-0.5	0.273
A12	1996	P127	0.8	0.437
A13	1983	P92	-0.2	-1.276
A13	2010	P147	-0.5	1.276
A16	1988	P108	1.7	0.587
A16	1989	P108	1.7	-0.494
A16	1989	P108	1.7	0.435
A16	2003	P143	-0.2	-0.384
A16	2005	P143	-0.2	0.087
A16	1995	P125	0.2	0.332
A16	1998	P133	0.3	0.166
A16	1993	P119	0	-0.869
A16	2011	N/A	N/A	2.276
A20	1997	P131	0.1	-1.446
A20	2003	P140	-0.3	1.446
A22	1997	P131	0.1	-0.282
A22	2003	P140	-0.3	0.282
I02	1995	P128	1.4	0.246
I02	2000	P133/P138	0.3/-0.1	-0.246
I03	1995	P126	0.6	0.328
I03	2003	P142	0.2	-0.328
I04	1995	P126	0.6	-0.274
I04	2003	P142	0.2	0.274
I05	1995	P126	0.6	0.836
I05	1995	P126	0.6	0.449
I05	2002	P140	-0.3	1.031
I05	1987	P97	2.1	-1.406
I05	2009	P149	0.8	0.234
I06	1993	P121	0.4	-0.264
I06	1996	N/A	N/A	-0.042
I06	2008	N/A	N/A	0.186
I08	1994	P124	0.6	-0.802
I08	1995	P126	0.6	0.479
I08	2007	P147	-0.5	0.206
I08	2007	P147	-0.5	0.802
I08	2000	P133/P138	0.3/-0.1	-0.563
I09	1995	P124	0.6	-0.338
I09	1995	P121/P123	0.4/0.7	N/A

I09	2004	P141	-0.3	0.338
IR6	1995	N/A	N/A	0.597
IR6	1995	N/A	N/A	0.828
IR6	2000	P133/P138	0.3/-0.1	-1.339
P01	1985	P96	2.5	1.154
P01	1999	P135	0.2	-0.680
P01	1999	P133/P134	0.3/0.3	0.385
P01	1999	P135	0.2	N/A
P01	1999	P133	0.3	-0.849
P01	2007	P148	0.2	-0.304
P01	2007	P148	0.2	-0.651
P02	1993	P123	0.7	1.175
P02	1994	P121	0.4	-2.600
P02	1994	P144	-0.5	-1.968
P02	1994	P144	-0.5	4.534
P02	2004	P144	-0.5	0.274
P02	1985	P96	2.5	0.956
P03	1985	P96	2.5	1.764
P03	2005	P145	-0.8	-1.553
P03	2006	P145	-0.8	N/A
P03	2005	P145	-0.8	-2.009
P06	1992	P116	1.4	-1.205
P06	1992	P116	1.4	0.357
P06	1992	P116	1.4	-1.167
P06	2003	P142	0.2	0.358
P06	2003	P142	0.2	-0.837
P06	2009	N/A	N/A	0.866
P09	1994	P123	0.7	-0.200
P09	2010	P152	N/A	0.200
P10	1993	P114/P120	2/-0.9	0.323
P10	2005	P145	-0.8	-0.323
P14	1993	P122	0.4	0.571
P14	1992	P120	-0.9	0.086
P14	2007	P148	0.2	-0.777
P14	2007	P148	0.2	-0.376
P15	1996	P114	2	-1.304
P15	2001	P140	-0.3	0.840
P15	2009	P148/P150	0.2/0.8	0.490
P16	1984	P92	-0.2	2.901
P16	1991	P114	2	0.932
P16	1991	P110	1.9	-1.431
P16	1991	P108/P114	1.7/2	0.010
P16	1992	P120	-0.9	0.222
P16	2006	P145	-0.8	-1.141
P16	2005	P144	-0.5	-0.319
P17	1991	P108/P114	1.7/2	-0.512
P17	1991	P120	-0.9	2.470

P17	1993	P122	0.4	0.915
P17	1992	P120	-0.9	0.460
P17	2001	P139	0.4	-1.754
P18	1994	P114	2	-0.209
P18	1994	P114	2	0.335
P18	2007	P147	-0.5	-0.483
P18	2008	P147	-0.5	0.209
P18	2006	P146	-1.2	N/A
P21	1994	P123	0.7	-0.447
P21	1994	P123	0.7	-0.240
P21	2009	P150	0.8	0.396
S01	1993	N/A	N/A	N/A
S01	1994	N/A	N/A	N/A
S01	1996	N/A	N/A	N/A
S03	1991	P115	2.5	N/A
S03	1995	P121/P123	0.4/0.7	-0.997
S03	1995	P128/P130	1.4/0.3	3.454
S03	1996	P128/P130	1.4/0.3	1.606
S03	2001	P113/P133/P137/P140	N/A/0.3/-0.4/-0.3	1.385
S03	1994	P121/P123/P137/P140	0.4/0.7/-0.4/-0.3	0.206
S03	1993	P121	0.4	-5.643
S03	2008	P140/P147/P148	-0.3/-0.5/0.2	0.884
S04	1989	P111	2.1	-0.703
S04	1990	P113	N/A	1.523
S04	1996	P127/P148	0.8/0.2	-1.893
S04	1998	P113	N/A	0.995
S04	1992	N/A	N/A	0.667
S04	2005	P144	-0.5	-0.716
S4P	1992	P108	1.7	0.059
S4P	2011	P152	N/A	-0.059

772

773

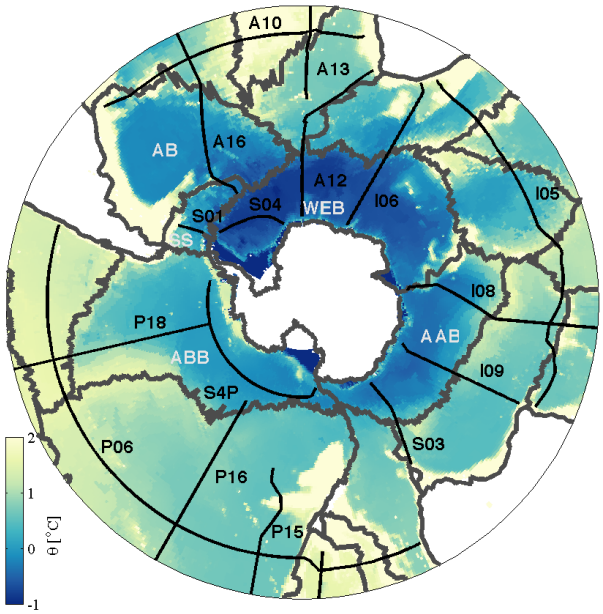

773

774 Fig. 1. Southern Ocean section locations (black lines) labeled with WOCE IDs (black
775 characters), indicating basin boundaries (gray lines) over bottom potential
776 temperature (color shading; Gourstski and Koltermann 2004) with land (white
777 shading). Basin names (white characters) are indicated by abbreviations including:
778 Weddell-Enderby Basin (WEB), Australian-Antarctic Basin (AAB), Amundsen-
779 Bellingshausen Basin (ABB), Scotia Sea (SS), and the Argentine Basin (AB).

780

781

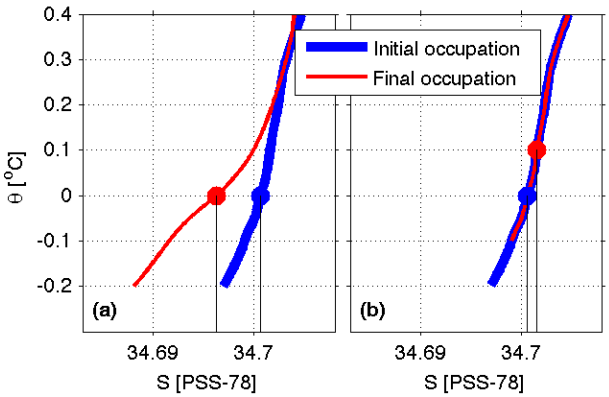

Figure 2: Schematics of changes in salinity between an initial (blue) and final (red) occupation of a given station owing to (a) water-mass change and (b) isotherm heave. Water-mass changes (a) can be seen as a change in the θ-S curve causing a deep freshening signal between occupations (black lines) at the same depths (dots). Isotherm heave (b), caused by a vertical displacement of potential isotherms, causes water at the same depth (dots) to warm and become more saline between occupations (black lines).

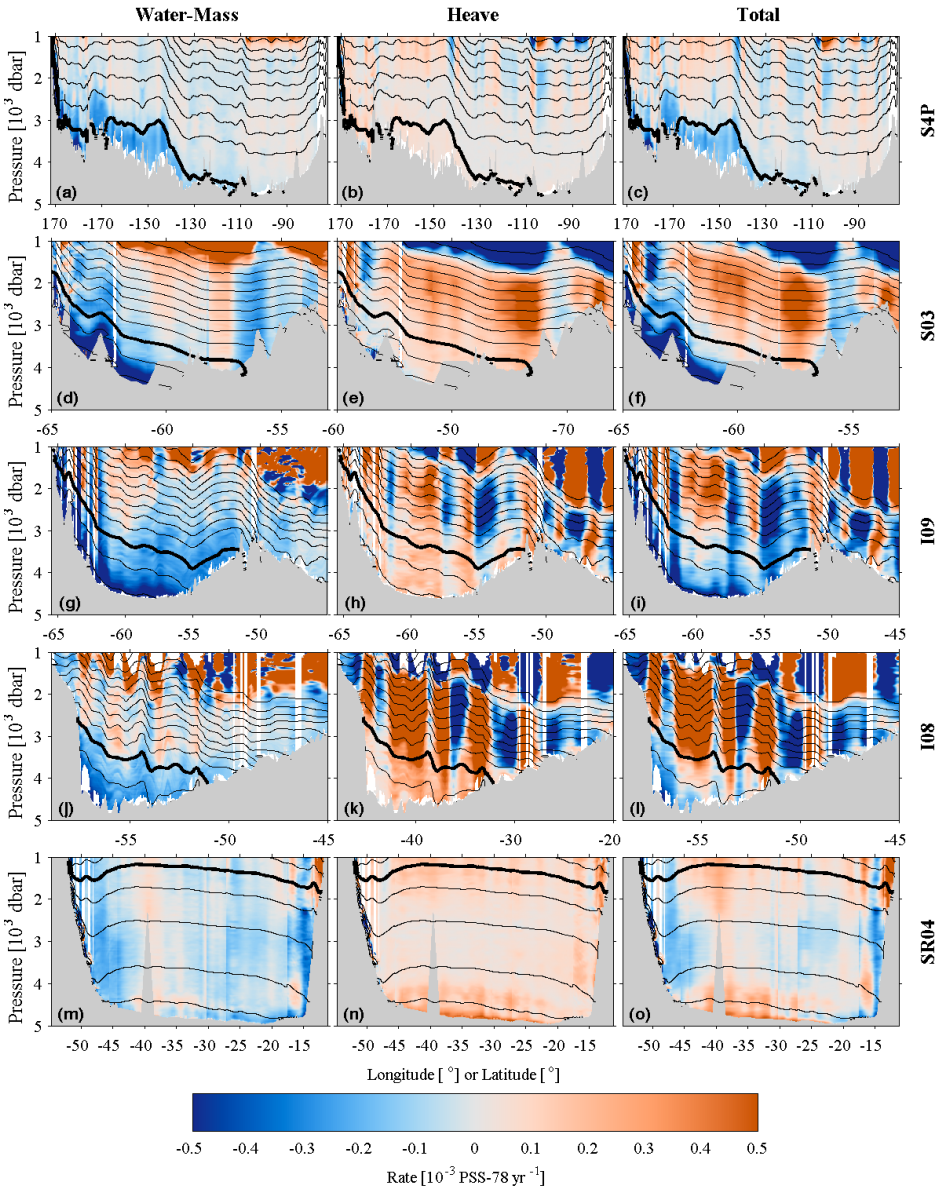

789

790 Fig. 3. Rate of change in S (color; in PSS-78 yr^{-1}) vs. pressure and latitude or
791 longitude along S4P (a-c), S03 (d-f) across the Australian-Antarctic Basin, I09 (g-i)
792 across the Australian-Antarctic Basin, I08 (j-l) across the Australian-Antarctic Basin,
793 and SR04 (m-o) across the Weddell Sea (see Fig.1 for locations). Orange indicates
794 areas of salinification and blue areas of freshening with mean isotherms contoured
795 at 0.2 °C intervals (thin black lines; 0°C isotherm thick black line). The water mass
796 (a, d, g, j, m) and heave (b,e,h,k,n) contributions to the total (c,f,i,l,o) are separated.

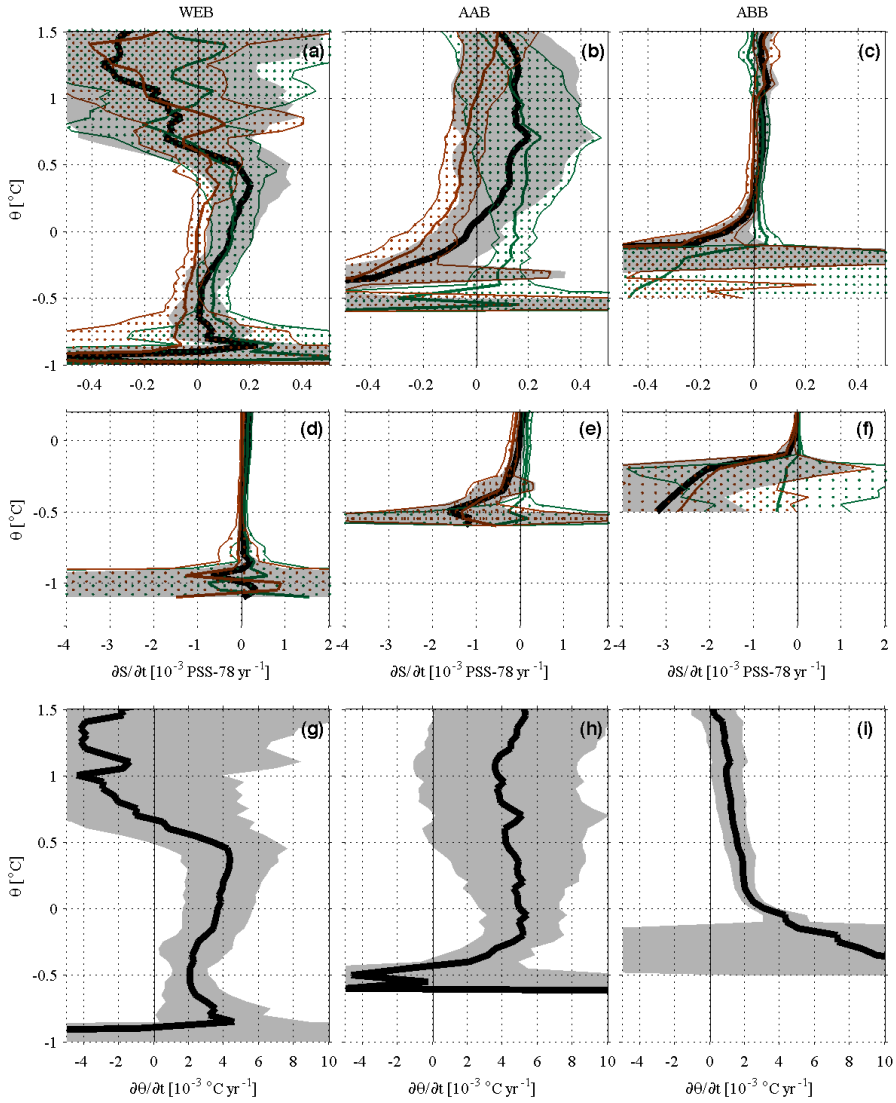

797

798 Figure 4: Basin-mean rates of change in S (black; a–f; PSS-78 yr^{-1}) and θ (black g–I;

799 °C yr^{-1}) with 95% confidence intervals (gray shading) estimated along time-mean θ

800 surfaces in the Weddell-Enderby Basin (WEB), Australian-Antarctic Basin (AAB) and

801 Amundsen- Bellingshausen Basin (ABB). The water-mass (red) and heave (green)

802 contributions to the total with 95% confidence intervals (dots) are shown over a

803 large θ range to show interior changes (a-c) as well as vertically expanded over a

804 limited θ range (d-f) to show large changes found in the coldest waters along the

805 continental slope (see Fig 3).

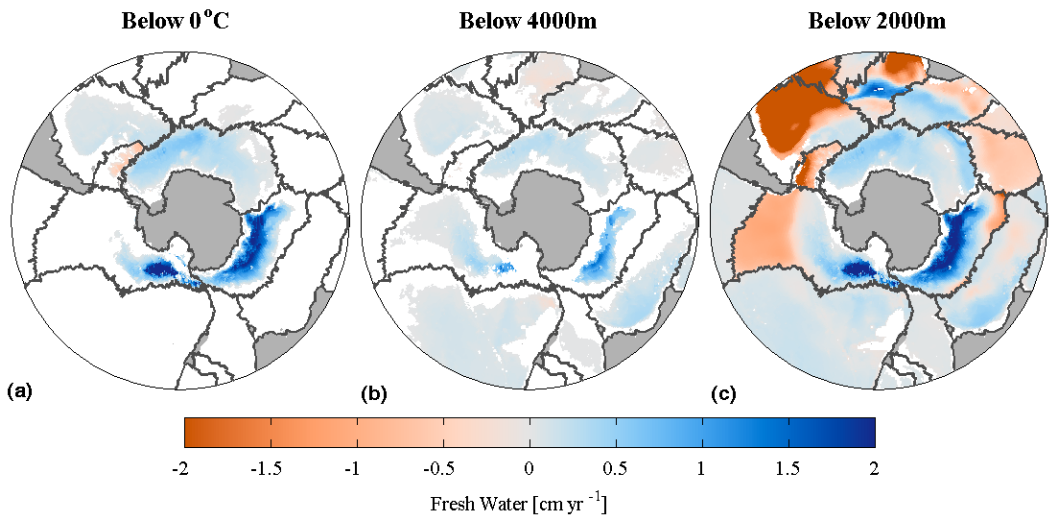

806

807

808 Figure 5. Local vertical column freshwater fluxes in cm yr^{-1} (color) below (a) 0°C, (b)

809 2000 m, and (c) 4000 m equivalent to observed water-mass salinity changes. Basin

810 boundaries (gray lines) and land (gray shading) are shown.

811

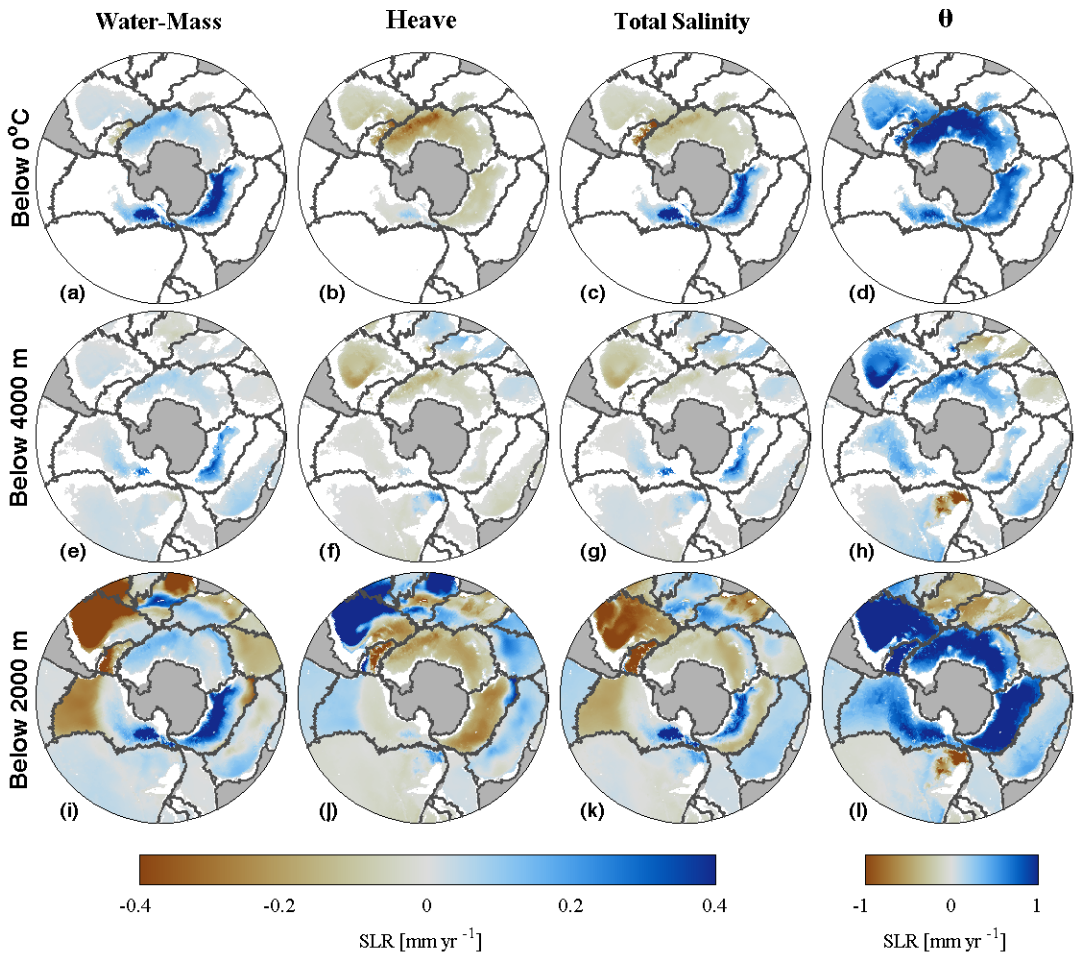

811

812 Figure 6: Vertical column total sea level rise [mm yr^{-1}] below θ = 0°C (a–d), 2000 m

813 (e–h) and 4000 m (i–l) owing to water-mass S changes (a,e,i), heave salinity changes

814 (b,f,j), net salinity changes (c,g,k), and θ changes (d,h,l). Brown indicates areas of

815 positive SLR and blue of negative SLR (see color legends). SLR is calculated based

816 on isotherm means within basin boundaries (gray lines; see Section 4).

817

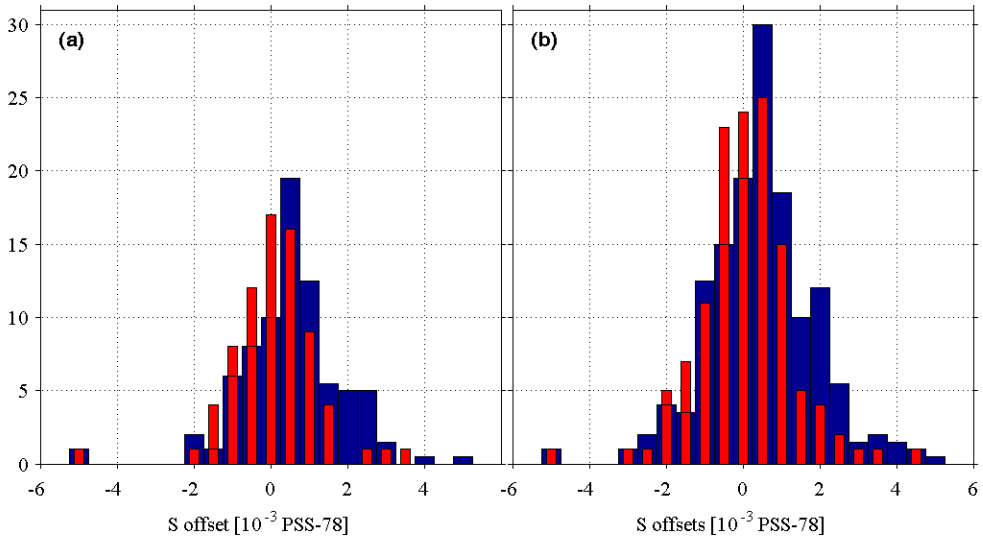

817

818 Figure A1: Histogram of estimated ad-hoc salinity offsets (red) and the sum of

819 recommended SSW batch and ad-hoc salinity offsets (blue) applied to the CTD data

820 along hydrographic legs in the (a) Southern Ocean and (b) Global Ocean (Table A1).

821 If a leg had more than one SSW batch offset, each offset is given an equal weight in

822 computing a mean.

823